Developments in the Built Environment 12 (2022) 100083

Contents lists available at ScienceDirect

Developments in the Built Environment

journal homepage: www.sciencedirect.com/journal/developments-in-the-built-environment

A simplified approach to evaluate cyclic response and seismic fragility of corrosion damaged RC bridge piers

Rajib Kumar Biswas [a,*], Mitsuyasu Iwanami [b], Nobuhiro Chijiwa [b], Takahiro Saito [a], Christian Malaga-Chuquitaype [c]

[a] Technical Research Institute, Okumura Corporation, 387, Osuna, Tsukuba, Ibaraki, 300-2612, Japan
[b] Department of Civil and Environmental Engineering, Tokyo Institute of Technology, Japan, 2-12-1-M1-21, O-okayama, Meguro, Tokyo, 152-8552, Japan
[c] South Kensington Campus, 322, Skempton Building, Imperial College London, United Kingdom

ARTICLE INFO

Keywords:
RC bridge Pier
Rebar corrosion
FEM analysis
Pushover analysis
Fragility analysis

ABSTRACT

Safety of the existing corrosion damaged reinforced concrete (RC) bridges during a seismic event is a matter of increasing concern. To reduce the enormous economic loss and casualties, it is important to examine the potential seismic risk of corroded RC bridge structures. This paper presents a simplified method to determine the seismic fragility of corroded RC bridge piers by developing a simplified FEM model and seismic fragility analysis. To make the proposed approach realistic, the numerical model is validated with two different experimental studies available in the literature. Obtain results from the simplified numerical model demonstrated excellent agreement with the experimental tests, making it suitable for seismic vulnerability analysis. After validation, the numerical model is further adopted to perform non-linear static pushover analysis of corroded RC bridge piers. Finally, a recently developed software tool SPO2FRAG is utilized to carry out seismic fragility analysis by defining three different damage levels.

1. Introduction

Corrosion of infrastructure is receiving particular attention, as it is associated with enormous economic loss. In a recent report, the global corrosion cost was estimated as $2.5 trillion in 2013. The amount was nearly 3.4% of the global gross domestic product. This report also indicated that up to 35% of the cost ($875 billion) could be saved by proper corrosion management practices (Bowman et al., 2016), (Khayatazad et al., 2020). According to another report, in the United States, approximately 87500 bridges (15% of the total amount) were reported as structurally deficient in 1997, mainly owing to steel bar corrosion that results in a cost of $8.3 billion (Koch et al., 2001). Meanwhile, in Japan, the annual average cost of corrosion of public infrastructure for the fiscal years 1996–1998 was JPY 207 billion (Survey of Corrosion Cost in, 1997).

Bridges are considered as crucial components for the national economy of a country. They play a key role in establishing a quick and reliable transportation system across the country and beyond. However, a seismic event may substantially damage the bridge structures (i.e., Kobe earthquake in 1995, Christchurch earthquake in 2011 etc.) and disrupt the transportation facilities as well as emergency and evacuation routes (Muntasir Billah and Shahria Alam, 2015). Therefore, it is important to understand the associated risk of existing deteriorated bridges to mitigate the enormous economic loss and casualties.

In recent times, several researchers started investigating the influence of rebar corrosion on the seismic fragility of RC structures (Zhong et al., 2012; Ghosh and Padgett, 2010; Choe et al., 2008, 2009; Dizaj et al., 2018). Zhong et al. (2012) developed fragility functions for the bridge structures incorporating the effect of rebar corrosion. Ghosh and Padget highlighted the effect of the aging of RC bridge piers on the seismic fragility. Choe et al., 2008, 2009 examined the adverse effect of rebar corrosion on the seismic fragility of single bent RC bridges. Dizaj et al. (2018) examined the seismic vulnerability of corroded RC frames considering non-uniform distribution of rebar corrosion. However, due to the increasing complexity of the existing approaches, an alternative simplified and reliable approach is needed that may help the infrastructure owner to estimate the associated risk of the infrastructure in a simplified manner.

* Corresponding author. Technical Research Institute, Okumura Corporation, 387, Osuna, Tsukuba, Ibaraki, 300-2612, Japan.
E-mail addresses: rajibkumar.biswas@okumuragumi.jp (R.K. Biswas), iwanami@cv.titech.ac.jp (M. Iwanami), chijiwa@cv.titech.ac.jp (N. Chijiwa), takahiro.saitoh@okumuragumi.jp (T. Saito), c.malaga@imperial.ac.uk (C. Malaga-Chuquitaype).

https://doi.org/10.1016/j.dibe.2022.100083
Received 21 June 2022; Received in revised form 25 July 2022; Accepted 2 August 2022
Available online 12 August 2022
2666-1659/© 2022 The Authors. Published by Elsevier Ltd. This is an open access article under the CC BY-NC-ND license (http://creativecommons.org/licenses/by-nc-nd/4.0/).

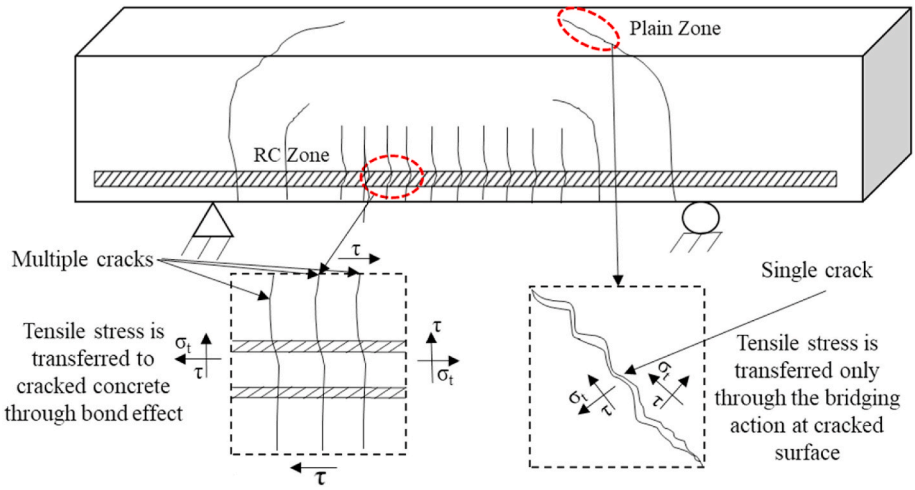

Fig. 1. RC and plain zone in concrete (Biswas et al., 2020a).

The novelty of this current work is that it presents a simplified approach for the probabilistic risk assessment of the corrosion damaged RC bridge piers by developing a simplified numerical model and using seismic fragility analysis. The simplified numerical model is developed following the author's previous advanced FEM model for RC beam (Biswas et al., 2020a) and column (Biswas et al., 2021a). The simplified FEM model is presented in Section 2. To avoid modeling burden and to make the numerical model simplified, the cross-sectional loss of the rebar is modelled in a uniform manner. When the RC bridge piers are subjected to low level of rebar corrosion (~5%), bond loss between the rebar and surrounding concrete is not considered. The reduced strength of the corrosion damaged concrete is modelled based on the study presented in (Shayanfar et al., 2016). In Section 3, to make the proposed approach realistic, the simplified FEM model is validated with two different experimental investigations (Guo et al., 2015) (Chang et al., 2019), where the RC bridge pier specimens were subjected to different levels of rebar corrosion. In Section 5, the simplified numerical model is adopted to carry out nonlinear static pushover analysis. Thereafter, the capacity curves obtained from the static pushover analysis is used as an input in the recently developed software tool SPO2FRAG (Baltzopoulos et al., 2017) and seismic fragility analysis is carried out for corroded RC bridge piers by defining three different damage levels namely damage level 1, damage level 2, and damage level 3. In Section 6, the important conclusions are summarized. The results obtained in this study will be useful to assess the potential seismic risk of the existing corroded RC bridge piers in a simplified way.

2. Simplified 3D FEM model

2.1. Modelling of concrete

Depending on the location of the rebar, the behavior of concrete will be different as demonstrated in Fig. 1. Concrete embedded with rebar is defined as a RC zone and concrete without any reinforcing bar is known as a plain concrete zone. The following equations represent the stress-strain relationships of RC and plain concrete zones (An et al., 1997; Maekawa et al., 2003).

$$\sigma_t = f_t\left(\frac{\varepsilon_{tu}}{\varepsilon_t}\right)^c \tag{1}$$

$$\int \sigma_t d\varepsilon_t = \int f_t \left(\frac{\varepsilon_{tu}}{\varepsilon_t}\right)^c d\varepsilon_t = \frac{G_f}{l_r} \tag{2}$$

Here, in Eq. (1), σ_t, ε_{tu}, f_t represents tensile stress, tensile strength, and cracking strain of concrete, respectively. In Eq. (2), c, ε_t, G_f, lr represents stiffening factor, average tensile strain of concrete, fracture energy, and mesh size.

2.1.1. Reduction of concrete strength

Owing to the expansion of corrosion product, concrete surrounding the corroded rebar is subjected to internal expansive pressure and it causes cracking in the surrounding concrete. Consequently, the effective compressive strength of the cracked concrete can be reduced substantially. In the numerical model, the reduction of compressive strength is considered following the experimental outcome of the study conducted by Shayanfar et al. (2016). The reduced compressive strength of concrete can be determined using the following equation.

$$f'_{c\_corroded} = (1-\lambda)^* f'_c \tag{3}$$

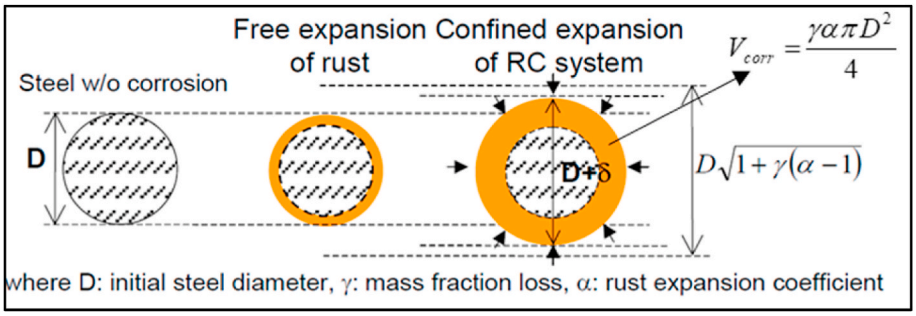

Fig. 2. Schematic representation of corrosion product in concrete (Toongoenthong and Maekawa, 2005).

where $f'_{c\_corroded}$ is reduced concrete compressive strength, λ denotes percent of compressive strength reduction, represents compressive strength of undamaged concrete.

For water to cement ratio of 0.5, λ can be calculated using following equation

$$\lambda = 2.576C_W - 1.876 \tag{4}$$

where C_W represents corrosion ratio of rebar.

2.2. Simulation of corrosion-related cracking in concrete

For effective modeling of corrosion-induced damage, it is important to consider corrosion-induced cracking (Yoon et al., 2000) (Coronelli and Gambarova, 2004). In the FEM analysis, corrosion-induced crack is modelled following the Toongoenthong-Maekawa model (Toongoenthong and Maekawa, 2005, 2007). Fig. 2 displays the schematic representation of the constitutive model. The average stiffness ($E_{s,eq}$) of the corroded system can be calculated by Eq. (5), where Υ,α, E_s and G represents volumetric loss of corroded rebar, coefficient related to corrosion product, volumetric loss of corroded rebar, stiffness of rebar and stiffness of rust product, respectively. Details can be found in (Yoon et al., 2000) and (Coronelli and Gambarova, 2004). It is noteworthy that, in the FEM analysis, the corrosion-induced stress is considered constant when the corrosion-induced crack reached the outer surface of the concrete (Biswas et al., 2019, 2021b).

$$E_{s,eq} = \frac{1+\gamma(\alpha-1)}{(1-\frac{\gamma}{E_s})+(\gamma\alpha/G)} \tag{5}$$

Temperature and oxygen level at the steel surface play important role for determining corrosion ratio (Rizwan and Ishida, 2011; Paul and van Zijl, 2017; Paul and van Zijl, 2016). In this numerical model, the effect of temperature and oxygen level is not considered to keep the numerical model simplified. Here, the accumulation of corrosion product around the rebar is considered uniform and the diameter of the corroded rebar is determined from the following equation,

$$D_{corrodedlayer} = D\sqrt{1+\gamma(\alpha-1)}$$

Here, α is the expansion coefficient of corroded substance, ϒ denotes the volume fraction loss of steel per unit and D represents the original steel diameter.

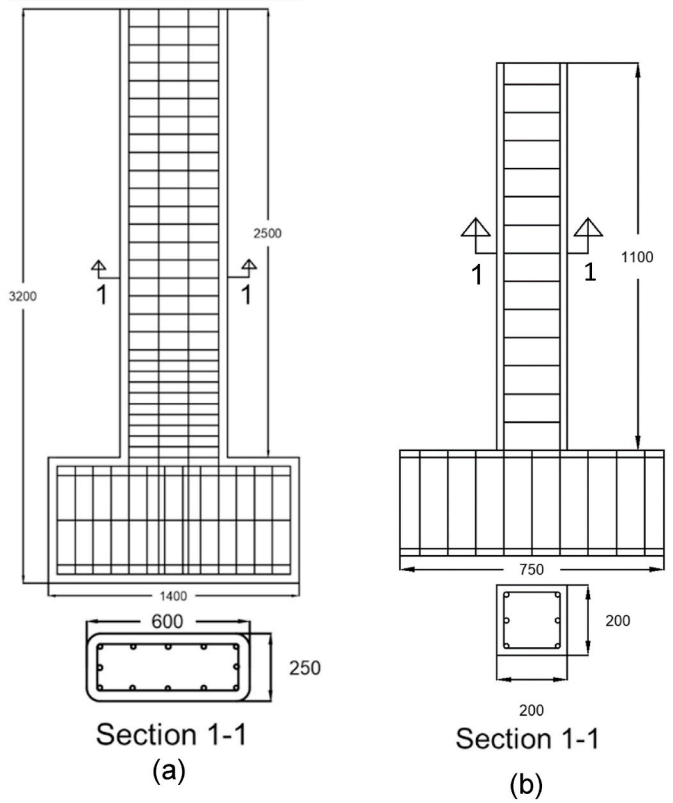

Fig. 3. Details of specimens (unit in mm) (a) Guo et al. (Guo et al., 2015) (b) Chang et al. (Chang et al., 2019).

2.3. Simulation of corroded rebar

Inside concrete, because of its high alkaline nature (pH value over 12), a dense passivating film forms around the rebars and provides a high level of corrosion protection (Talakokula et al., 2016). However, when the pH value becomes lower or there is ingress of deleterious element (Cl^-) from the environment, the passivating film becomes unstable and rebar corrosion initiates (Andrade, 2021) (Gao et al., 2021).

Steel bar corrosion may occur mainly in two categories i.e. chloride induced and carbonation induced corrosion. Carbonation induced corrosion generally leads to uniform corrosion, whether, chloride induced corrosion results in non-uniform corrosion. In FEM analysis, one of the major difficulties is to represent the non-uniform distribution of rebar corrosion. Often it may become a modeling burden. To make the FEM analysis simple, the corroded rebar is modelled in a uniform manner. Here, a probabilistic model is used (Choe et al., 2008, 2009) to represent uniform corrosion.

2.3.1. Corrosion initiation phase

If the chloride concentration around the embedded rebar reaches the threshold value, steel bar corrosion initiates. The rebar corrosion initiation time can be determined using the following equation ,

$$T_{corr} = X_1\left\{\frac{d^2{}_c}{4k_e\,k_t\,k_c\,D_0 t^n{}_0}\left[erf^{-1}\left(\frac{C_s - C_{cr}}{C_s}\right)\right]^{-2}\right\}^{\frac{1}{1-n}} \tag{6}$$

Here, X_1 represents uncertainty factor of model, d_c represents depth of concrete cover, k_e denotes environmental factor, k_t is test factor, k_c represents curing factor, D_0 denotes diffusion coefficient, t_0 is reference period, n represents age factor. C_{cr} is critical chloride concertation and C_s represents equilibrium chloride concentration. erf^{-1} denotes Gaussian error function.

2.3.2. Corrosion propagation phase

After the initiation of steel bar corrosion, it starts progressing with time. In the corrosion propagation phase, the level of rebar corrosion can be determined from the following equations ,

$$D_{corr} = D_s - \frac{1.05081(1-\frac{w}{c})^{-1.64}}{D_{corr}} * (t - T_{corr})^{0.71} \tag{7}$$

where D_{corr} and D_s represent diameter of corroded and sound steel bars. w/c is water to cement ratio. T_{corr} is starting time of steel bar corrosion, t represents time after corrosion initiates.

$$X_{corr} = \frac{D_s{}^2 - D_{corr}{}^2}{D_o{}^2} * 100 \tag{8}$$

where X_{corr} represents the degree of rebar corrosion.

If experimental results of the corroded rebars are available, the corrosion ratio can be determined using the calculations below.

$$A_S(X_{corr}) = \frac{\pi D^2}{4}\left(1 - \frac{X_{corr}}{100}\right) \tag{9}$$

$$X_{corr} = \frac{W_s - W_{corr}}{W_s} * 100 \tag{10}$$

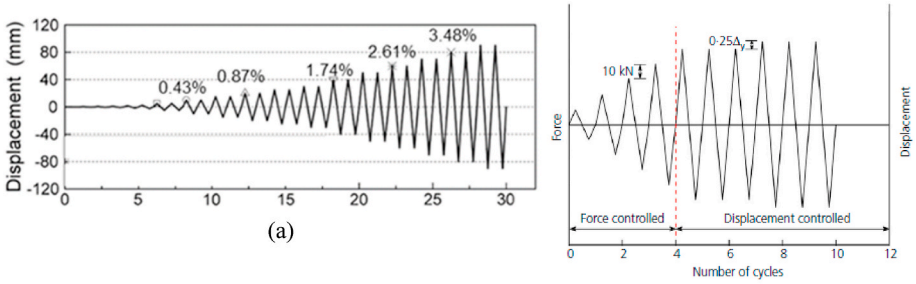

Fig. 4. Loading history used in the experimental studies (a) Guo et al. (Guo et al., 2015) (b) Chang et al. (Chang et al., 2019).

where W_s and W_{corr} represent weight of non-corroded and corroded reinforcements, X_{corr} denotes corrosion ratio.

2.4. Modelling of bond deterioration

When rebar corrosion begins, corrosion products expand in volume, causing tensile stress on the nearby concrete. As corrosion amount reaches a critical limit, cracks occur along with the rebar and as a result, the reinforcing bar and the concrete become separated. In the FEM analysis of this study, bond loss among rebar and concrete is represented by corrosion-induced cracking (Toongoenthong and Maekawa, 2005). It is reported in the literature that the bond strength may slightly increase when the RC member is subjected to low level of corrosion (Almusallam et al., 1996; Kearsley and Joyce, 2014; Coccia and Imperatore, 2014). Almusallam et al. (1996) reported that bond strength can be increased when the corrosion ratio is up to 4%. Thus, it can be considered that a low level of corrosion may not influence the bond strength substantially. To make the numerical modeling simplified and reduce the modeling burden, the bond deterioration was not considered in this study for slightly corroded specimens (~5% corrosion).

3. Reference experimental tests

To investigate the effect of rebar corrosion on the cyclic response of RC bridge piers, Guo et al. (2015) carried out reversed cyclic loading tests of RC bridge piers with different degrees of rebar corrosion. Four single shaft RC bridge piers were casted and the height of the column pier was 2500 mm with a cross-section of 250 x 600 mm. The specimen was casted on a 1400 x 1400 × 700 mm foundation (see Fig. 3). The bridge piers were reinforced with 16 mm diameter rebar and the longitudinal reinforcement ratio was 1.61%. 8 mm diameter rebar was used as transverse reinforcement. The transverse reinforcement ratio was 1.42% at the bottom 600 mm of the pier; however, it was reduced to 0.58% at the remaining part of the pier. The longitudinal and transverse reinforcements had yield strengths of 362 MPa and 325 MPa, respectively. During reversed cyclic loading, first, a 514 kN axial load was applied gradually to the sound and corroded specimens, afterward, displacement controlled reverse cyclic loading was carried out. The loading history of the reversed cyclic loading can be seen in Fig. 4(a). The horizontal load was applied at a height of 2300 mm. Depending on the degree of corrosion, corroded RC bridge piers can be categorized into three different zones, i.e., splash and tidal zone, submerged zone, and atmospheric zone. Normally, splash and tidal zone is subjected to higher degree of corrosion owing to drying-wetting cycles and higher chloride concentration. Considering this fact, only 500 mm above the foundation was subjected to an accelerated corrosion process. A total of four bridge piers were tested in this study, where Specimen 1 was the control specimen. The average corrosion ratio of the longitudinal rebars of Specimen 2, 3, and 4 was 5.07%, 9.74%, and 15.24%, respectively. In contrast to the sound specimen, Specimen 2, 3, and 4 demonstrated 20.2%, 20.9%, 37.6% less yield, and 20.8%, 27.5%, 35.2% less maximum load-carrying capacity respectively in the positive loading cycle.

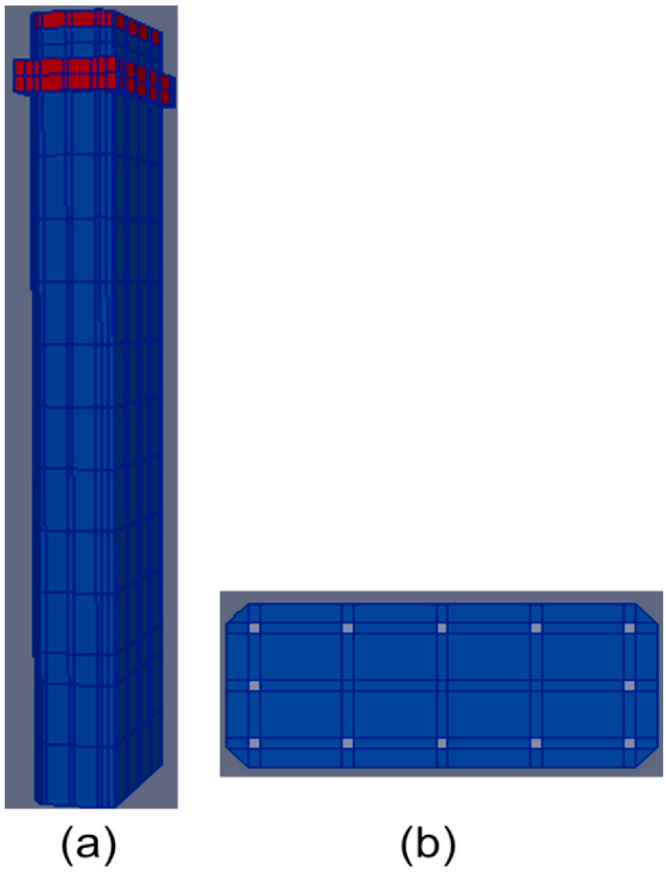

Fig. 5. Analysis model of RC bridge piers (a) 3D view (b) top view.

To further investigate the accuracy of the simplified numerical model, and to predict the structural behavior of RC columns with low level of rebar corrosion, another experimental study conducted by Chang et al. (2019) was considered. Out of the ten tested specimens, two specimens (XZ-6 & XZ-7) subjected to low level of rebar corrosion were selected. The columns were casted with 200 × 200 mm cross-section and a length of 1100 mm (see Fig. 3). The effective length of the column was 900 mm with an aspect ratio of 4.5. The columns were reinforced with a 14 mm steel bar and the longitudinal reinforcement ratio was 2.31%. 6 mm rebar was used as transverse reinforcement with a center to center spacing of 80 mm. Specimens XZ-6 & XZ-7 were subjected to steel bar corrosion ratio of 5.57% and 4.06% and axial load of 0 and 249 kN respectively. The reversed cyclic loading history of this experimental study is shown in Fig. 4(b).

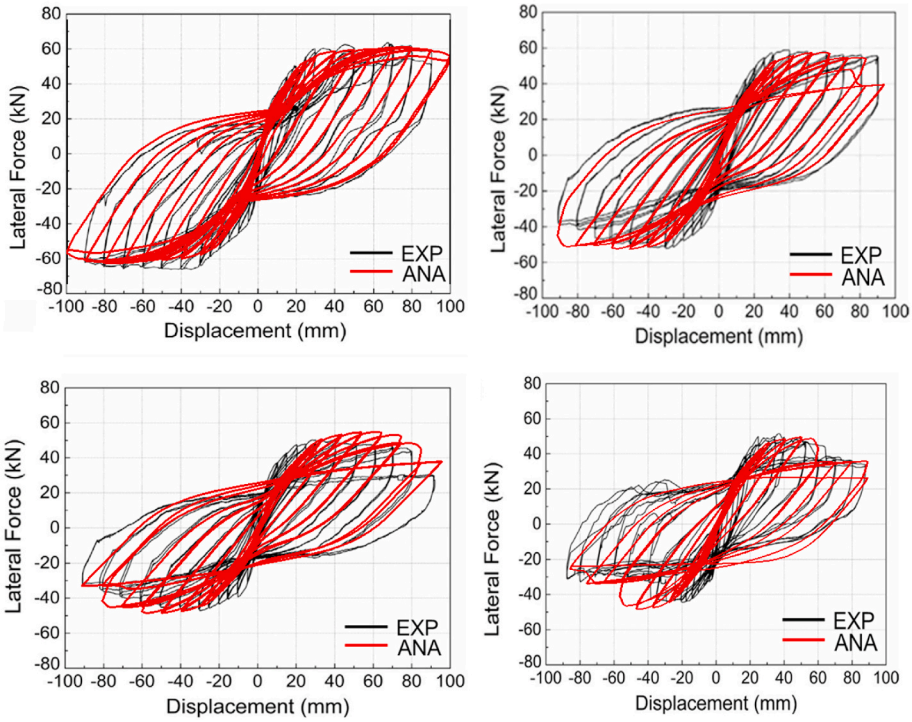

Fig. 6. Comparison of hysteresis loop (a) Sound specimen (Guo et al., 2015) (b) Specimen 2 (Guo et al., 2015) (c) Specimen 3 (Guo et al., 2015) (d) Specimen 4 (Guo et al., 2015).

4. Validation of the simplified numerical model

Finite element software package COM 3 was used to perform reversed cyclic loading of the corroded specimens using the proposed simplified model. The reliability of this software tool can be found elsewhere (Chijiwa and Maekawa, 2015a, 2015b; Uno et al., 2017; Kurihara et al., 2017; Chijiwa et al., 2018; Yamada et al., 2017). Modelling of the foundation part of the RC bridge pier was omitted (see Fig. 5) as no damage was reported in the experimental study. RC and plain concrete zones were modelled based on the availability of steel bar as described in *Section 2.1*. Corrosion induced cracking was modelled only for the longitudinal reinforcement. The phenomena of rebar corrosion were modelled in two steps. In the first step, rust product, crack propagation and corrosion induced stress were modelled following Toogoenthong-Maekawa model (Toongoenthong and Maekawa, 2005, 2007). Thereafter, once the corrosion induced crack reached the concrete surface, the reduced reinforcement ratio was modelled in a uniform manner. Since the failure mode of the specimen was governed by flexure, and to obtain simplicity, corrosion induced cracking and rust growth were not considered for the transverse reinforcement and reduced reinforcement ratio was inserted in the mesh uniformly. The bond between rebar and concrete was modelled by using corrosion induced cracking, following Toogoenthong-Maekawa model (Toongoenthong and Maekawa, 2005, 2007). The bond deterioration was only considered for highly corroded cases.

In all three directions, all nodes at the bottom of the specimen were constrained to restrict the rotation and displacement during reversed cyclic loading. To avoid local failure at the loading points, steel plates were installed to distribute the loading stress uniformly. The original Newton-Raphson iterative method was used to conduct the FEM analysis and the number of iterations was set sufficiently large to obtain stable convergence. In the FEM analysis, the reversed cyclic loading was conducted at displacement levels of 10, 20, 30, 40, 50, 60, 70, 90, and 100 mm.

The global behaviors of the specimens obtained from the numerical analysis are compared with experimental results in Fig. 6. The difference between the maximum load-carrying capacities for sound specimens is less than 11% in both loading cycles (positive and negative). Specimen 2 had lower level of rebar corrosion (5.07%). Therefore, in the numerical analysis, corrosion-induced damage and bond loss between steel bar and surrounding concrete were not considered. Nevertheless, there was an excellent correlation in the global response. In both loading cycles, the discrepancy between the maximum load-carrying capacity in the experimental and numerical studies was less than 5%. In Specimens 3 and 4, this difference was calculated as less than 7% in both loading cycles. It is noteworthy that, in terms of maximum load carrying capacity, obtained results provided better prediction than the other simplified models (Rao et al., 2017; Lepech et al., 2015) available in the literature.

Table 1
Comparison of failure displacement.

Specimen	Failure displacement (positive direction, Exp.)	Failure displacement (negative direction, Exp.)	Failure displacement (Both direction, FEM)
Specimen 1	>90 mm	>90 mm	100 mm
Specimen 2	71.5 mm	90 mm	80 mm
Specimen 3	58.4 mm	60.8 mm	70 mm
Specimen 4	41.8 mm	60.1 mm	60 mm

Table 1 compares the failure displacements obtained from the experimental study and numerical analysis. Here, the failure displacement was termed as a 15% reduction in maximum load-carrying capacity. As shown in Table 1, the simplified numerical model was able to predict the failure displacement with high precision. For example, in Specimen 2, the failure displacement was obtained as 90.1 mm and 71.5 mm in negative and positive loading cycles. The simplified numerical model may slightly overestimate the displacement capacity of highly corroded RC bridges as can be seen in Table 1. The slight discrepancies

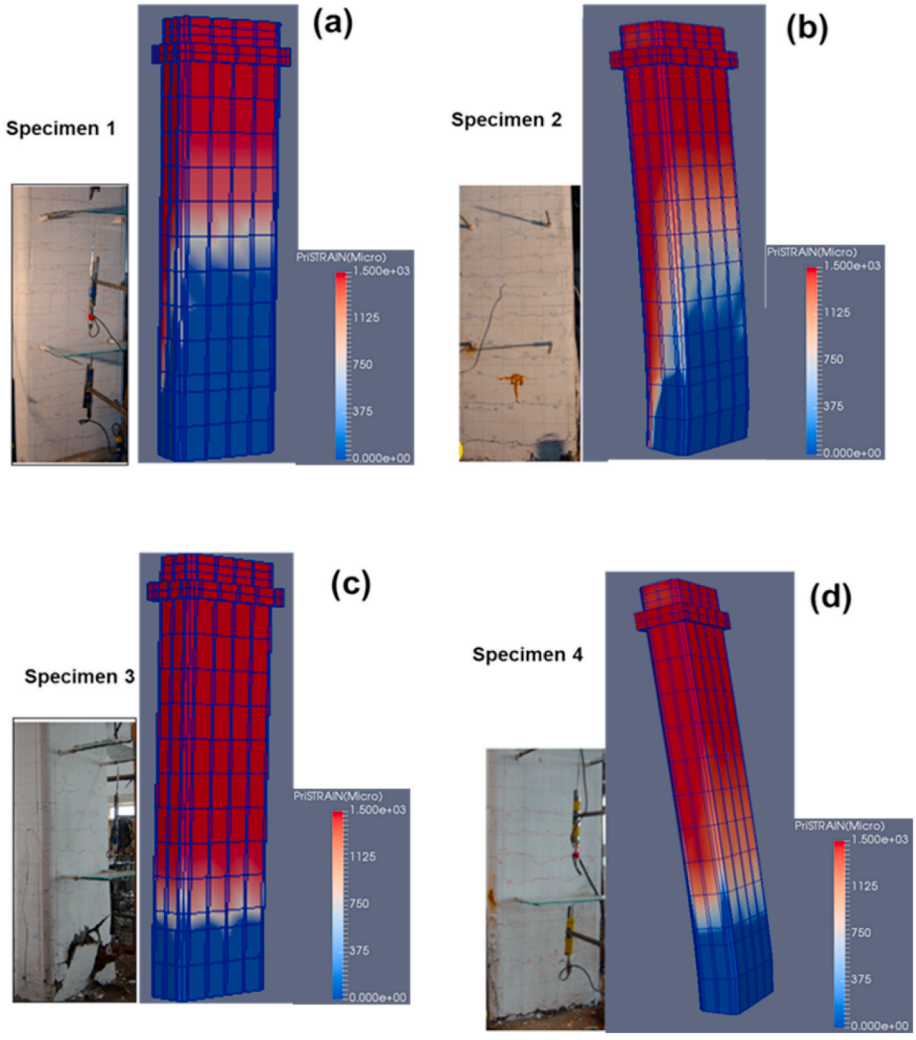

Fig. 7. Comparison of cracking pattern and strain distribution(a) Sound specimen (b) Specimen 2 (c) Specimen 3 (d) Specimen 4.

between the experimental and numerical analysis were indeed expected and it can be attributed to the consideration of uniform corrosion in the FEM analysis. Highly corroded bridge piers can be subjected to non-uniform corrosion with corrosion pit which was not considered in the simplified FEM model.

Rebar corrosion significantly affects the structural behavior of RC structures (Berto et al., 2009; Crespi et al., 2020; Crespi et al., 2022; G. M. et al., 2018) and it is important to consider mechanical damages caused by corrosion products and related cracking in the surrounding concrete (Coronelli and Gambarova, 2004). In the simplified FEM model, corrosion substance and corrosion induced cracking were considered when the corrosion ratio is more than 5%. The experimental study carried out by Guo et al. (2015) reported that the failure of the RC bridge piers was governed by flexure. To reduce the modelling burden, corrosion products and corrosion induced cracking effect are considered only for the main reinforcing bars, and corrosion effect in the stirrup is considered only by reducing the cross-sectional area of the rebar. However, a similar failure pattern can be seen in the numerical analysis

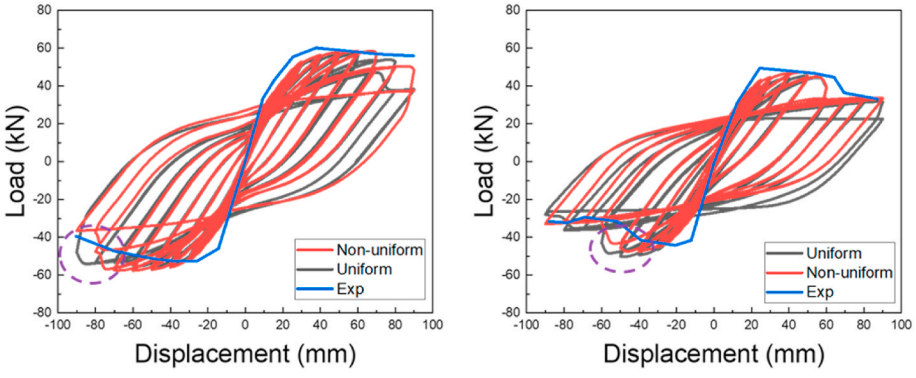

Fig. 8. Comparison of different kinds of analysis and experimental results.

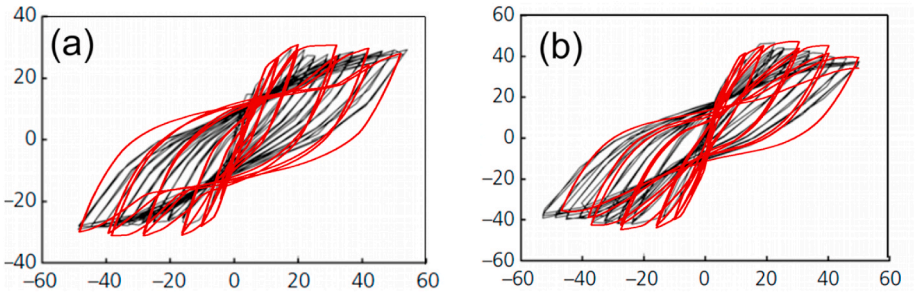

Fig. 9. Comparison of hysteresis loops (a) XZ-6 (b) XZ-7.

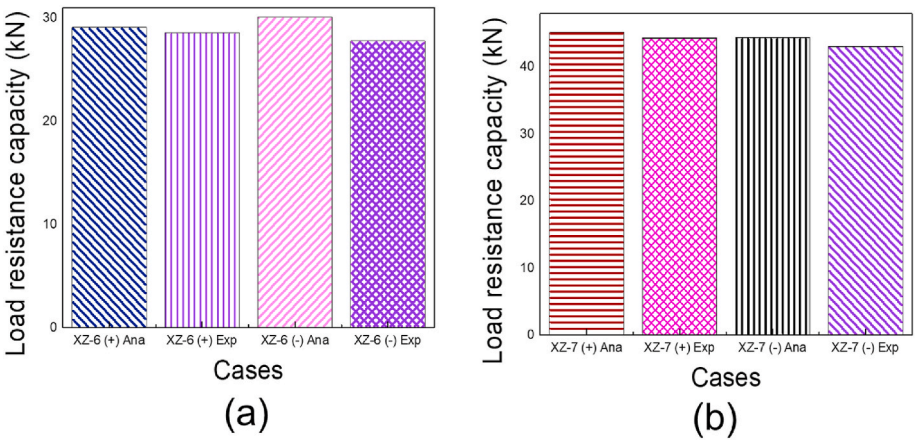

Fig. 10. Comparison of maximum load carrying capacity between experimental and numerical study in the positive and negative cycles (a) XZ-6 (b) XZ-7.

with the simplified numerical model as shown in Fig. 7. Flexural cracks were observed up to 1200 mm from the bottom of the sound specimen. The simplified numerical model well captured the failure mode and crack distribution. Specimen 2 also exhibited similar behavior to Specimen 1. The crack direction and crack length were well captured in the numerical simulation. It is noteworthy that smeared crack model is considered for the numerical analysis and in Fig. 7 cracks are presented in micro-strain unit.

In Specimens 3 and 4, owing to high average corrosion ratio, the damage was concentrated at the bottom of the specimen. The FEM analysis was able to capture this phenomenon with good correlation.

It is clear from Figs. 6 and 7 and above discussion that the proposed model was able to capture the structural behaviour in terms of maximum load-carrying capacity, crack pattern, crack length, initial stiffness, and displacement capacity even though a simplified numerical model with uniform corrosion distribution was adopted. To understand the difference between the simplified numerical model with uniform corrosion distribution and a detailed FEM model (Biswas et al., 2020a) with non-uniform rebar corrosion, numerical analyses were conducted on the specimen with low and high levels of rebar corrosion (Specimens 2 and 4), and obtained results are compared in Fig. 8. In FEM analysis, non-uniform corrosion was modelled for all individual steel bar. Here, the maximum and minimum length of the mesh in the specimen axis was 200 mm and 100 mm, respectively. Interestingly, the predicted displacement capacity and load carrying capacity in the both negative and positive loading cycles from the detailed FEM model had a marginal difference with the simplified approach, as indicated in Fig. 8.

To further verify the simplified model without considering the bond deterioration and non-uniform corrosion, the structural behaviour of two specimens with a low level of rebar corrosion was analyzed. Two specimens (XZ-6 and XZ-7) were considered from the experimental study carried out by Chang et al. (2019). In numerical analysis, the cyclic loading was conducted at displacement levels of 8, 16, 24, 32, and

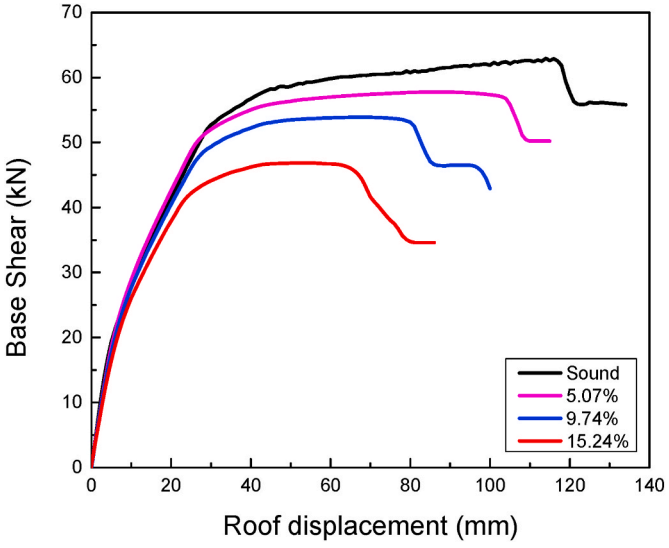

Fig. 11. Capacity curves of sound and corroded specimen.

48 mm. The comparison of the experimental and the FEM analysis can be seen in Figs. 9 and 10. It can be seen that the simplified numerical model without considering non-uniform corrosion and bond deterioration was able to predict the load bearing behaviour with high precision. For Specimen XZ-6, the difference between the maximum load-carrying capacity in the experimental and numerical study is less than 8% in both loading cycles. In the case of Specimen XZ-7, the difference was calculated as less than 3% in both loading cycles.

Thus, in light of the obtained results from the simplified numerical model, it can be considered suitable for assessment of seismic

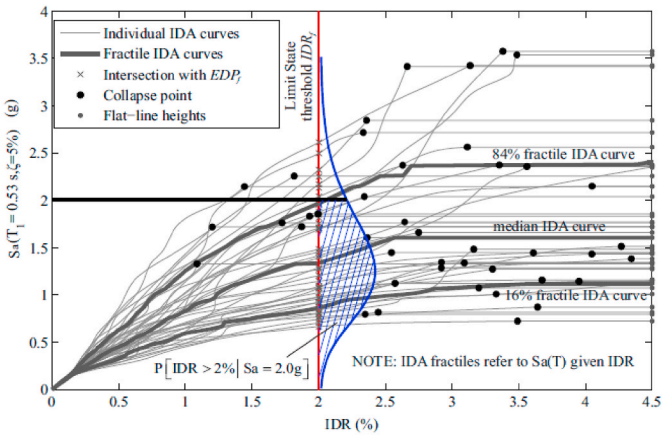

Fig. 12. Illustration of structural fragility analysis using incremental dynamic analysis (Baltzopoulos et al., 2017).

vulnerability of corroded RC bridge piers.

5. Assessment of seismic vulnerability of corrosion damaged RC bridge piers

5.1. Pushover analysis

Pushover analysis is a non-linear static (NLS) analysis where the structures are subjected to monotonically increasing lateral load and constant axial load simulating the inertia load that the structure would encounter during a seismic event. In this analysis, the response of the structure can be specified by the capacity curve that defines the relationship between top displacement and base shear.

Pushover analysis was carried out in COM 3 for the sound and corroded RC bridge piers tested by Guo et al. (2015). The capacity curves generated from the pushover analysis are shown in Fig. 11. Several important observations can be noted from the NLS pushover analysis. As can be seen in Fig. 11, the sound specimen was able to withstand considerably high base shear than the corroded specimens. The base shear capacity of the RC bridge piers decreased substantially as the corrosion ratio increased. In comparison to the undamaged specimen, Specimen 2, 3, and 4 demonstrated 6.4%, 12.9%, and 25.8% reduced base shear capacity, respectively. The corroded RC bridge specimens also demonstrated significantly less drift capacity than the sound specimens. Specimen 2, 3, and 4 demonstrated 16.3%, 30.3%, and 46.7% less drift capacity than the sound specimen. Also, it can be noted that initial stiffness slightly decreased with the increase of corrosion ratio.

5.2. Seismic fragility analysis

Seismic fragility analysis (SFA) represents the probability of exceeding a predefined damage limit state for a particular structure at a defined seismic intensity level. Incremental dynamic analysis (IDA), proposed by Vamvatsikos and Cornell (Vamvatsikos and Allin, 2002) is a widely adopted method to determine the seismic fragility of a given structure. In IDA, structures are subjected to a set of ground motions scaled to the increased level of seismic intensity to explore the structural behavior at various seismic intensity levels. In this approach, the behavior of the structure is generally represented by engineering demand parameters (EDP) such as the maximum drift ratio or inter-story drift ratio. Seismic intensity is represented by the peak ground acceleration (PGA) or spectral acceleration in the first mode, Sa (T1). Fig. 12 illustrates an example of structural fragility analysis using incremental dynamic analysis. In general, a logarithmic distribution is assumed and IDA curves at 16%, 50%, and 84% fractile are used to obtain the mean and standard deviation. Using the IDA framework, fragility curves can be defined using a lognormal cumulative distribution function as.

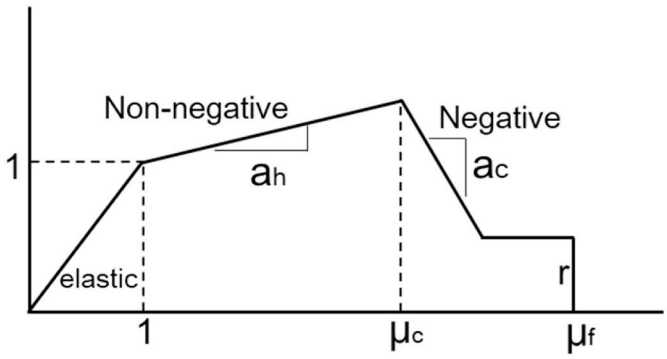

Fig. 13. Quadrilinear backbone curve for seismic fragility analysis.

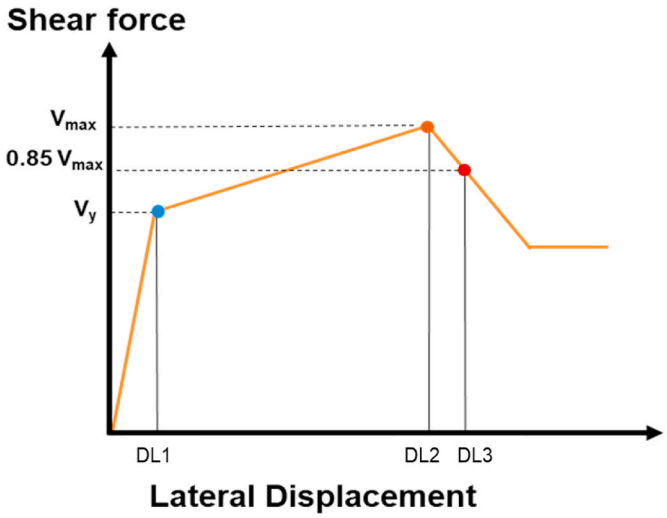

Fig. 14. Limit states for SFA of RC bridge piers.

$$P[\mathrm{IM}_f^{LS} \le im] = \Phi[\frac{\ln(im) - \eta}{\beta}] \tag{11}$$

where η represents mean and β is logarithmic standard deviation.

Different approaches that use capacity curve of the structure to estimate the seismic fragility curves at various limit state are available in the literature, for e.g., SPO2FRAG (Baltzopoulos et al., 2017), Malla and Wijeyewickrema (2022), Han and Chopra (Han et al., 2010), Dolsek and Fajfar (2021). However, in this study, a widely used software package SPO2FRAG (Baltzopoulos et al., 2017) was used to carry out SFA of sound and corroded RC bridge piers. It is a simpler alternative to dynamic analysis-based seismic fragility analysis. In SPO2FRAG, using the quadrilinear backbone curve as illustrated in Fig. 13, a set of semi-empirical analytical equations developed by Vamvatsikos and Cornell (2006) are utilized to predict the median and variability of peak seismic response of the SDOF system. The backbone curve having four different segments has an elastic start, and it yields at the ductility with $\mu = 1$. Then it hardens at a slope a_h, afterward it turns negative with a slope a_c. Finally, it achieves a residual strength of height r. Details can be found in (Vamvatsikos and Cornell, 2006).

To estimate the seismic fragility, the pushover curves shown in Fig. 11 are used as an input parameter. After that, the software converts the pushover curves to a quadrilinear model following the method proposed by De Luca et al. (De Luca et al., 2013) and serves as input for fragility analysis. Three different limit states are considered in this study

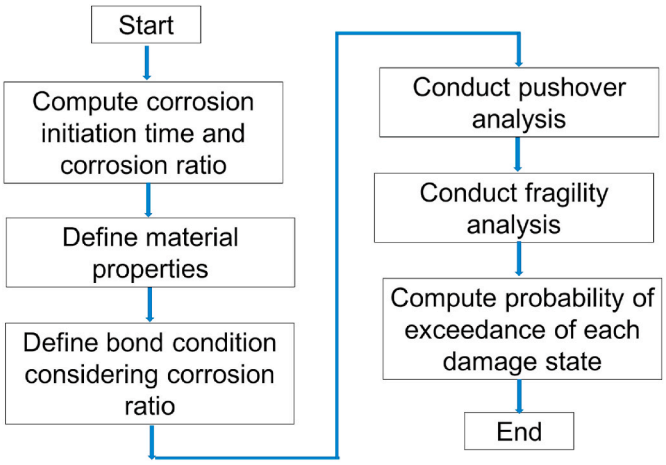

Fig. 15. Flow chart of simplified seismic fragility analysis of corroded RC bridge piers.

for seismic fragility analysis as shown in Fig. 14.

- Damage level 1 (DL1) is considered as the lateral displacement corresponding to the yield displacement of the RC bridge pier. Similar consideration can be also seen in the literature (Xu et al., 2020).
- Damage level 2 (DL2) is defined as the displacement corresponding the maximum strength of the RC bridge pier as considered in (Xu et al., 2020; Goksu, 2021).
- Damage level 3 (DL3) is considered as the commonly considered the failure displacement corresponding to decrease of lateral strength to 85% of the maximum strength (Li et al., 2018).

5.3. *Effect of corrosion damage on the seismic fragility of RC bridge piers*

Fig. 15 presents a flow chart that depicts a concise overview of the simplified approach of fragility analysis of the corroded RC bridge pier. As a first major step, corrosion initiation time and corrosion ratio need to be estimated. Thereafter, the material properties of the corroded RC bridge piers should be determined. Then, as a second major step, pushover analysis of the RC corroded bridge pier should be carried out and capacity curves need to be established. Thereafter, based on the obtained capacity curves, SFA can be carried out. After that, the probability of exceedance of each damage state can be obtained. Fig. 16 displays the fragility curves for different damage states and corrosion levels. As shown in Fig. 16 (a), rebar corrosion did not have a significant influence on DL1. This can be attributed to the fact that the sound and corroded bridge piers attain DL1 at considerably low level of ground motion intensities and thus the effect of corrosion is not reflected. Similar phenomena can also be noticed in the literature (Xu et al., 2020).

The influence of rebar corrosion becomes pronounced at DL2. For example, for an acceleration of 0.6g, the probability of exceedance was about 30% for sound RC bridge piers. However, the probability of exceedance significantly increased to about 44%, 60%, and 84% for RC bridge piers with 5.07%, 9.74%, and 15.24% rebar corrosion, respectively. This represents that for an acceleration of 0.6g probability of exceedance was increased by 31.8%, 50.0% 64.2% corresponding to corrosion ratios of 5.07%, 9.74%, and 15.24%, respectively. This behavior is indeed expected since the displacement ductility of the

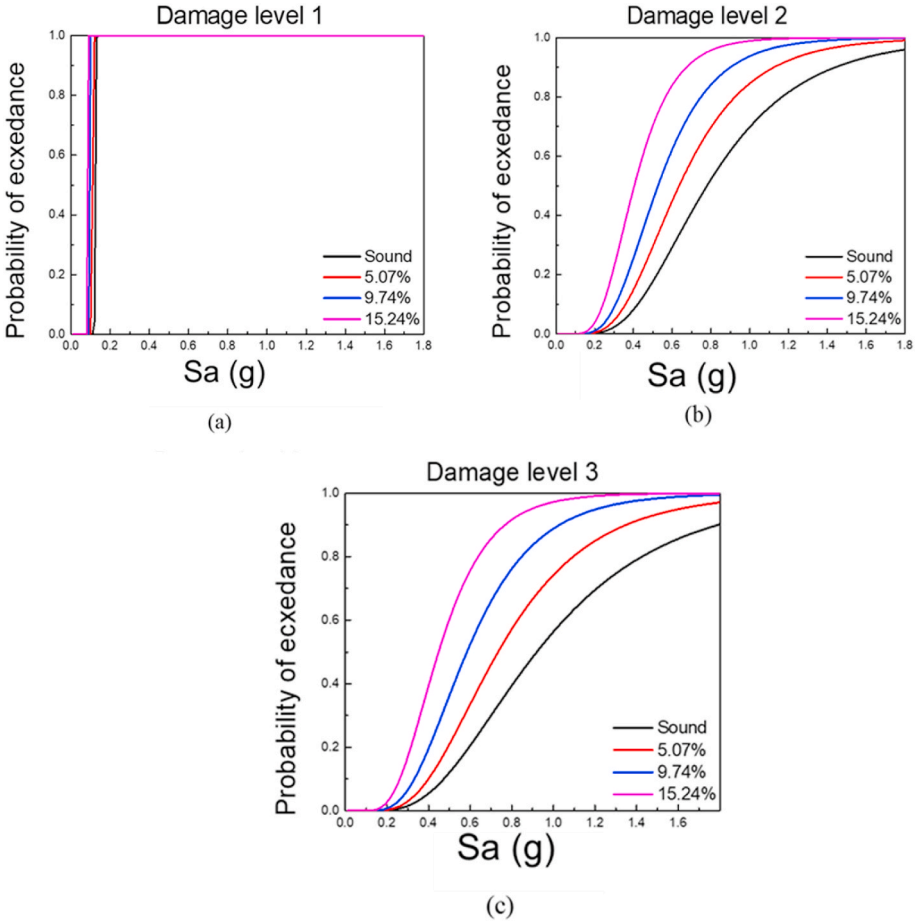

Fig. 16. Fragility curves for different damage states and corrosion levels.

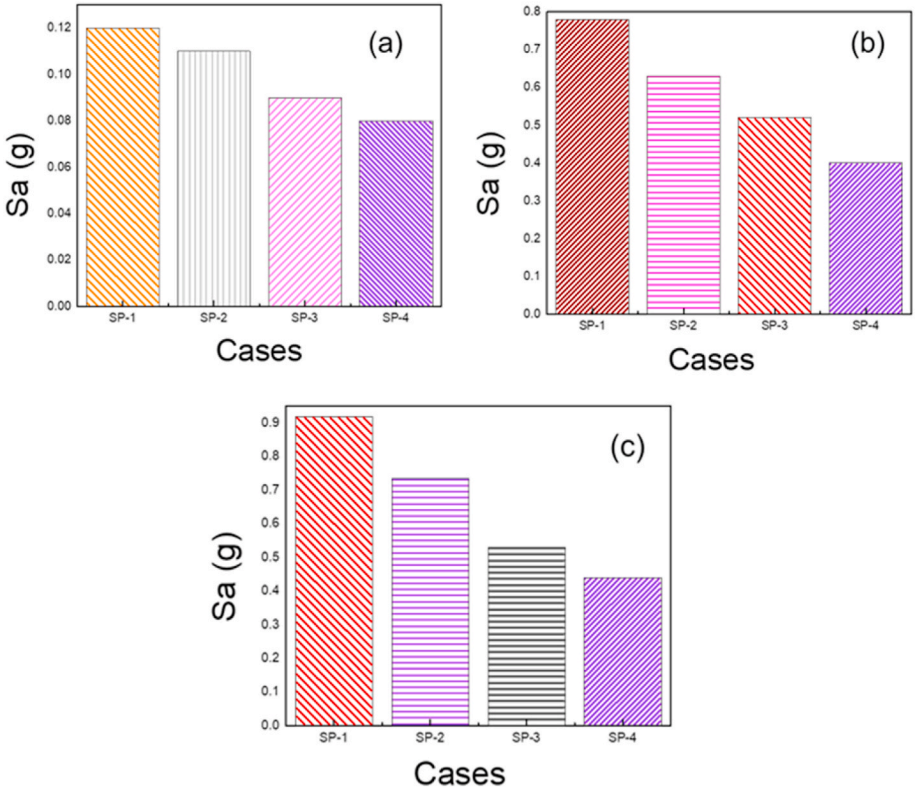

Fig. 17. Comparison between median values of spectral acceleration for probability of exceedance for (a) DL1 (b) DL2 (c) DL3.

corroded RC bridge piers decreased substantially with the increase of corrosion ratio. Similar to DL2, rebar corrosion also had a significant impact on the probability of exceeding the damage limit state in DL3. For example, to obtain a 60%probability exceedance, the required ground acceleration was 1.03g for the undamaged RC bridge pier specimen. However, the corresponding ground acceleration was 0.81g, 0.6g, and 0.44g for the specimen with rebar corrosion of 5.07%, 9.74%, and 15.24% rebar corrosion, representing an increase of 21.3%, 41.7%, and 57.2% respectively.

Fig. 17 depicts the median values of spectral acceleration (g) for each damage level. It can be seen that median values of the Sa (g) reduced remarkably with the increase of corrosion ratio. In DL2, the median Sa (g) for the sound case was determined as 0.78g, whereas the median for Specimen 4 was obtained as 0.4g. Similarly, in DL3, the median Sa (g) for the sound case was determined as 0.92g, while the median for Specimen 4 was obtained as 0.44g. This behavior can be attributed to the less displacement capacity of the corroded specimens.

6. Conclusions

This research presents a simplified approach to estimate seismic fragility of corrosion damaged RC bridge piers by developing a simplified 3D numerical model to predict the structural behavior of corroded RC bridge piers. To make the proposed approach realistic, the numerical model was validated with two different experimental studies available in the literature, where RC bridge piers or columns were subjected to various degrees of rebar corrosion. After validation of the FEM model, it was adopted to carry out the nonlinear static pushover analysis. Thereafter, based on the non-linear static pushover analysis, seismic fragility analysis was carried out by defining three different damage levels. Following are some key conclusions that can be drawn from the findings of this study.

- The proposed simplified 3D dimensional FEM model was capable to capture the structural response of corroded RC bridge piers in terms of initial stiffness, maximum load-carrying capacity, and cracking pattern.
- The numerically obtained results validated with experimental studies demonstrated that rebar corrosion significantly affected the load-bearing capacity and ductility of RC bridge piers. A similar tendency was also observed in the NLS pushover analysis.
- Seismic fragility analysis was carried out for the sound and corroded RC bridge pier specimens indicated that an increased amount of rebar corrosion significantly increases the probability of exceedance in the respective damage level.
- Neglecting the extent of rebar corrosion might result in a substantial underestimation of the potential risk of structural damage to corroded RC bridge piers.

Funding

This research did not receive any specific grant from funding agencies in the public, commercial, or not-for-profit sectors.

Declaration of competing interest

The authors declare that they have no known competing financial interests or personal relationships that could have appeared to influence the work reported in this paper.

References

Almusallam, A.A., Al-Gahtani, A.S., Aziz, A.R., 1996. Rasheeduzzafar, Effect of reinforcement corrosion on bond strength. Constr. Anad Build. Mater. 10, 123–129 papers3://publication/uuid/E4C9EF72-4BBD-4C8A-928A-1697F37B93B1.

An, X., Maekawa, K., Okamura, H., 1997. Numerical simulation of size effect in shear strength of RC beams. J. Mater. Concr. Struct. Pavement, JSCE. 35, 297–316. https://doi.org/10.2208/jscej.1997.564_297.

Andrade, C., 2021. Developments in the Built Environment Chloride ingress rate and threshold content , as determined by the ' Integral ' test method. In: In Concrete with Several W/C Ratios in Saturated and Unsaturated Conditions, vol. 8. https://doi.org/10.1016/j.dibe.2021.100062.

Baltzopoulos, G., Baraschino, R., Iervolino, I., Vamvatsikos, D., 2017. SPO2FRAG: software for seismic fragility assessment based on static pushover. Bull. Earthq. Eng. 15, 4399–4425. https://doi.org/10.1007/s10518-017-0145-3.

Berto, L., Vitaliani, R., Saetta, A., Simioni, P., 2009. Seismic assessment of existing RC structures affected by degradation phenomena. Struct. Saf. 31, 284–297. https://doi.org/10.1016/j.strusafe.2008.09.006.

Biswas, R.K., Iwanami, M., Chijiwa, N., Uno, K., 2019. Finite element analysis of rc beams subjected to non-uniform corrosion of steel bars. Sustain. Constr. Mater. Technol.

Biswas, R.K., Iwanami, M., Chijiwa, N., Uno, K., 2020. Effect of non-uniform rebar corrosion on structural performance of RC structures: a numerical and experimental investigation. Construct. Build. Mater. 230 https://doi.org/10.1016/j.conbuildmat.2019.116908.

Biswas, R.K., Iwanami, M., Chijiwa, N., Nakayama, K., 2021. Structural assessment of the coupled influence of corrosion damage and seismic force on the cyclic behaviour of RC columns. Construct. Build. Mater. 304, 124706 https://doi.org/10.1016/j.conbuildmat.2021.124706.

Biswas, R.K., Iwanami, M., Chijiwa, N., Nakayama, K., 2021. Numerical evaluation on the effect of steel bar corrosion on the cyclic behaviour of RC bridge piers. Mater. Today Proc. 44, 2393–2398. https://doi.org/10.1016/j.matpr.2020.12.453.

Bowman, E., Jacobson, G., Koch, G., Varney, J., Thopson, N., Moghissi, O., Gould, M., Payer, J., 2016. International Measures of Prevention, Application, and Economics of Corrosion Technologies Study. NACE Int.. A-19.

Chang, Z., Xing, G., Luo, D., Liu, B., 2019. Seismic behavior and strength prediction of corroded RC columns subjected to cyclic loading. Mag. Concr. Res. 1–53. https://doi.org/10.1680/jmacr.18.00181.

Chijiwa, N., Maekawa, K., 2015. Thermo-hygral case-study on full scale rc building under corrosive environment and seismic actions. J. Adv. Concr. Technol. 13, 438–448. https://doi.org/10.3151/jact.13.465.

Chijiwa, N., Maekawa, K., 2015. Thermo-Hygral case-study on full scale RC building under corrosive environment and seismic actions. J. Adv. Concr. Technol. 13, 465–478. https://doi.org/10.3151/jact.13.465.

Chijiwa, N., Hayasaka, S., Maekawa, K., 2018. Long-term differential and averaged deformation of box-type pre-stressed concrete exposed to natural environment. J. Adv. Concr. Technol. 16, 1–17. https://doi.org/10.3151/jact.16.1.

Choe, D.E., Gardoni, P., Rosowsky, D., Haukaas, T., 2008. Probabilistic capacity models and seismic fragility estimates for RC columns subject to corrosion. Reliab. Eng. Syst. Saf. 93, 383–393. https://doi.org/10.1016/j.ress.2006.12.015.

Choe, D.-E., Gardoni, P., Rosowsky, D., Haukaas, T., 2009. Seismic fragility estimates for reinforced concrete bridges subject to corrosion. Struct. Saf. 31, 275–283.

Coccia, S., Imperatore, S., 2014. Influence of Corrosion on the Bond Strength of Steel Rebars in Concrete. https://doi.org/10.1617/s11527-014-0518-x.

Coronelli, D., Gambarova, P., 2004. Structural assessment of corroded reinforced concrete beams: modeling guidelines. J. Struct. Eng. 130, 1214–1224. https://doi.org/10.1061/(ASCE)0733-9445 (2004)130:8(1214).

Crespi, P., Zucca, M., Valente, M., 2020. On the collapse evaluation of existing RC bridges exposed to corrosion under horizontal loads. Eng. Fail. Anal. 116, 104727 https://doi.org/10.1016/j.engfailanal.2020.104727.

Crespi, P., Zucca, M., Valente, M., Longarini, N., 2022. Influence of corrosion effects on the seismic capacity of existing RC bridges. Eng. Fail. Anal. 140, 106546 https://doi.org/10.1016/j.engfailanal.2022.106546.

De Luca, F., Vamvatsikos, D., Iervolino, I., 2013. Near-optimal piecewise linear fits of static pushover capacity curves for equivalent SDOF analysis. Earthq. Eng. Struct. Dynam. 42, 523–543. https://doi.org/10.1002/eqe.

Dizaj, E.A., Madandoust, R., Kashani, M.M., 2018. Probabilistic seismic vulnerability analysis of corroded reinforced concrete frames including spatial variability of pitting corrosion. Soil Dynam. Earthq. Eng. 114, 97–112. https://doi.org/10.1016/j.soildyn.2018.07.013.

Fajfar, P., 2021. Simplified Probabilistic Seismic Performance Assessment of Plan-Asymmetric Buildings ‡, pp. 2021–2041. https://doi.org/10.1002/eqe.

Gao, Y., Suryanto, B., Chai, H.K., Forde, M.C., 2021. Developments in the Built Environment Evaluating the effect of corrosion on shear-critical RC beams by integrated NDT. Dev. Built Environ. 7, 100050 https://doi.org/10.1016/j.dibe.2021.100050.

Ghosh, J., Padgett, J.E., 2010. Aging considerations in the development of time-dependent seismic fragility curves. J. Struct. Eng. 136, 1497–1511. https://doi.org/10.1061/(ASCE)ST.1943-541X.0000260.

G.M., Antonio Bossio, F.B., Fabbrocino, Francesco, Monetta, Tullio, , Gian Piero Lignola, Prota, Andrea, 2018. Corrosion effects on seismic capacity of reinforced concrete structures. Corrosion Rev. 44.

Goksu, C., 2021. Fragility functions for reinforced concrete columns incorporating recycled aggregates. Eng. Struct. 233, 111908 https://doi.org/10.1016/j.engstruct.2021.111908.

Guo, A., Li, H., Ba, X., Guan, X., Li, H., 2015. Experimental investigation on the cyclic performance of reinforced concrete piers with chloride-induced corrosion in marine environment. Eng. Struct. 105, 1–11. https://doi.org/10.1016/j.engstruct.2015.09.031.

Han, S.W., Moon, K., Chopra, A.K., 2010. Application of MPA to Estimate Probability of Collapse of Structures, pp. 1259–1278. https://doi.org/10.1002/eqe.

Kearsley, E.P., Joyce, A., 2014. Effect of corrosion products on bond strength and flexural behaviour of reinforced concrete. slabs 56, 21–29.

Khayatazad, M., De Pue, L., De Waele, W., 2020. Developments in the Built Environment Detection of corrosion on steel structures using automated image processing. Dev. Built Environ. 3, 100022 https://doi.org/10.1016/j.dibe.2020.100022.

Koch, G.H., Brongers, M.P.H., Thompson, N.G., Virmani, Y.P., Payer, J.H., 2001. Corrosion Cost and Preventive Strategies, Corrosion. 202, p. 1. –16. http://watermainbreakclock.com/docs/techbrief.pdf.

Kurihara, R., Chijiwa, N., Maekawa, K., 2017. Thermo-hygral analysis on long-Term natural frequency of RC buildings with different dimensions. J. Adv. Concr. Technol. 15, 381–396. https://doi.org/10.3151/jact.15.381.

Lepech, M.D., Rao, A., Kiremidjian, A., Michel, A., Stang, H., Geiker, M., 2015. Multi-physical and multi-scale deterioration modelling of reinforced concrete part II: coupling corrosion and damage at the structural scale. Concr. - Innov. Des. Fib Symp. Proc. 307–308.

Li, D., Wei, R., Xing, F., Sui, L., Zhou, Y., Wang, W., 2018. Influence of Non-uniform corrosion of steel bars on the seismic behavior of reinforced concrete columns. Construct. Build. Mater. 167, 20–32. https://doi.org/10.1016/j.conbuildmat.2018.01.149.

Maekawa, K., Pimanmas, A., Okamura, H., 2003. Nonlinear Mechanics of Reinforced Concrete. Spon Press, London.

Malla, N., Wijeyewickrema, A.C., 2022. Collapse assessment of low-rise reinforced concrete special moment resisting frame systems using a simplified method. Structures 38, 1–13. https://doi.org/10.1016/j.istruc.2022.01.076.

Muntasir Billah, A.H.M., Shahria Alam, M., 2015. Seismic fragility assessment of highway bridges: a state-of-the-art review. Struct. Infrastruct. Eng. 11, 804–832. https://doi.org/10.1080/15732479.2014.912243.

Paul, S.C., van Zijl, G.P.A.G., 2016. Chloride-induced corrosion modelling of cracked reinforced SHCC. Arch. Civ. Mech. Eng. 16, 734–742. https://doi.org/10.1016/j.acme.2016.04.016.

Paul, S.C., van Zijl, G.P.A.G., 2017. Corrosion deterioration of steel in cracked SHCC. Int. J. Concr. Struct. Mater. 11, 557–572. https://doi.org/10.1007/s40069-017-0205-8.

Rao, A.S., Lepech, M.D., Kiremidjian, A.S., Sun, X.Y., 2017. Simplified structural deterioration model for reinforced concrete bridge piers under cyclic loading1. Struct. Infrastruct. Eng. 13, 55–66. https://doi.org/10.1080/15732479.2016.1198402.

Rizwan, R., Ishida, T., 2011. Enhanced electro-chemical corrosion model for reinforced concrete under severe coupled action of chloride and temperature. Construct. Build. Mater. 25, 1305–1315. https://doi.org/10.1016/j.conbuildmat.2010.09.014.

Shayanfar, M.A., Barkhordari, M.A., Ghanooni-Bagha, M., 2016. Effect of longitudinal rebar corrosion on the compressive strength reduction of concrete in reinforced concrete structure. Adv. Struct. Eng. 19, 897–907. https://doi.org/10.1177/1369433216630367.

Survey of Corrosion Cost in Japan, 1997. Tokyo Japan Soc. Corros. Eng. Japan Assoc. Corros. Control, pp. 1–33. https://doi.org/10.1177/0272431613483005.

Talakokula, V., Bhalla, S., Ball, R.J., Bowen, C.R., Pesce, G.L., Kurchania, R., Bhattacharjee, B., Gupta, A., Paine, K., 2016. Sensors and Actuators A : physical Diagnosis of carbonation induced corrosion initiation and progression in reinforced concrete structures using piezo-impedance transducers. Sensor Actuator Phys. 242, 79–91. https://doi.org/10.1016/j.sna.2016.02.033.

Toongoenthong, K., Maekawa, K., 2005. Simulation of coupled corrosive product formation, migration into crack and propagation in reinforced concrete sections. J. Adv. Concr. Technol. 3, 253–265. https://doi.org/10.3151/jact.3.253.

Toongoenthong, K., Maekawa, K., 2007. Multi-mechanical approach to structural performance assessment of corroded RC members in shear. J. Adv. Concr. Technol. 3, 107–122. https://doi.org/10.3151/jact.3.107.

Uno, K., Chijiwa, N., Iwanami, M., Miyoshi, T., Ogasawara, Tetsuya, 2017. Evaluation of residual structural performance of steel pipe piled pier with local steel bar corrosion. Ocean Eng. 73.

Vamvatsikos, D., Allin, C.C., 2002. Earthquake engineering and structural dynamics. Earthq. Eng. Struct. Dynam. 31, 491–14.

Vamvatsikos, D., Cornell, C.A., 2006. Direct Estimation of the Seismic Demand and Capacity of Oscillators with Multi-Linear Static Pushovers, pp. 1097–1117. https://doi.org/10.1002/eqe.573.

Xu, J.G., Wu, G., Feng, D.C., Cotsovos, D.M., Lu, Y., 2020. Seismic fragility analysis of shear-critical concrete columns considering corrosion induced deterioration effects. Soil Dynam. Earthq. Eng. 134, 106165 https://doi.org/10.1016/j.soildyn.2020.106165.

Yamada, Y., Chijiwa, N., Iwanami, M., 2017. Effect of artificial crack length along tensile rebar on fatigue load carrying mechanism of RC beams without stirrups. Mater. Concr. Struct. JSCE. 73, 323–336.

Yoon, S., Wang, K., Weiss, W.J., Shah, S.P., 2000. Interaction between loading, corrosion, and serviceability of reinforced concrete. ACI Struct. J. 97, 637–644. https://doi.org/10.14359/9977.

Zhong, J., Gardoni, P., Rosowsky, D., 2012. Seismic fragility estimates for corroding reinforced concrete bridges. Struct. Infrastruct. Eng. 8, 55–69. https://doi.org/10.1080/15732470903241881.